International Journal of Refrigeration 99 (2019) 300–315

Contents lists available at ScienceDirect

International Journal of Refrigeration

journal homepage: www.elsevier.com/locate/ijrefrig

Numerical (CFD) and experimental analysis of hybrid household refrigerator including thermoelectric and vapour compression cooling systems

Engin Söylemez[a,*], Emre Alpman[b], Ayhan Onat[c], Yalçin Yükselentürk[b], Selim Hartomacıoğlu[c]

[a] Faculty of Mechanical Engineering, BSH Bosch, Marmara University, Turkey
[b] Faculty of Engineering, Department of Mechanical Engineering, Marmara University, Istanbul, Turkey
[c] Faculty of Technology, Department of Mechanical Engineering, Marmara University, Istanbul, Turkey

ARTICLE INFO

Article history:
Received 4 September 2018
Revised 28 November 2018
Accepted 3 January 2019
Available online 5 January 2019

Keywords:
Cooling
CFD analysis
Energy consumption
Refrigerator
Thermoelectric cooler
Vapour compression

ABSTRACT

Numerical and experimental analysis of a previously investigated hybrid household refrigerator (HHR), HHR I, were conducted in this study. To determine the optimum location for the thermoelectric cooler installed in HHR I, CFD analysis was performed. As a result of the CFD predictions, two new HHRs, namely HHR II and III, were created and experimentally investigated.

CFD predictions showed a more uniform air velocity and temperature distributions inside the fresh food compartments of HHR II and III compared to HHR I. Additionally, experimental measurements indicated a considerable increase in the energy efficiency of HHR II and III. Their energy consumption was nearly identical and improvements of up to 10% and 27% at the ambient temperatures of 16 °C and 32 °C, respectively, were observed when compared to HHR I. Regarding the cooling time, no effect of the relocation of the TEC was observed at the TEC's nominal voltage of 24 V.

© 2019 Elsevier Ltd and IIR. All rights reserved.

Analyse numérique (CFD) et expérimentale d'un réfrigérateur domestique hybride intégrant des systèmes de refroidissement thermoélectriques et à compression de vapeur

Mots-clés: Refroidissement; Analyse CFD; Consommation énergétique; Réfrigérateur; Refroidisseur thermoélectrique; Compression de vapeur

1. Introduction

1.1. Previous TEC based refrigerator studies

Interest in and experiments in the application of thermoelectric coolers (TECs) in household refrigerators are steadily increasing. In comparison with compressor-based vapour compression (VC) technologies, TECs' are compact and have fewer components (thus, less maintenance needs). However, more efforts are needed to increase their coefficient of performance (COP) values which are low in comparison to VC technologies (Hermes and Barbosa, 2012; Bansal and Martin, 2000). The works by Vian and Astrain (2009a) and Astrain et al. (2012) focused on the energy consumption of hybrid refrigerators combining TE and VC cooling technologies as well as developing a computational model for the simulation of the complete hybrid refrigerator. In another experimental study, Astrain et al. (2016) investigated the effect of different heat exchange systems (water–air heat exchanger, finned heat sink, and heat pipes) on the efficiency of a thermoelectric refrigerator. Their study showed that higher COP values for TE refrigerators can be achieved through the optimal design of the heat

* Corresponding author.
E-mail address: Engin.Soylemez@Bshg.com (E. Söylemez).

https://doi.org/10.1016/j.ijrefrig.2019.01.007
0140-7007/© 2019 Elsevier Ltd and IIR. All rights reserved.

Nomenclature

ANN	Artificial Neural Network
CC	chill compartment
CFD	computational fluid dynamics
Comp	compressor
COP	coefficient of performance (WW^{-1})
CRO	chemical reaction optimisation
Cu	copper
DC	direct current (A)
EEC	energy efficiency class
FC	freezer compartment
FEM	finite element method
FFC	fresh food compartment
Gr_L	Grashof number
HHR	hybrid household refrigerator
IEC	International Electrotechnical Commission
IV	idling voltage (V)
Ma	Mach number
Nu	Nusselt number
POD	proper Orthogonal Decomposition
Pr	Prandtl number
Ra_L	Rayleigh number
RPM	revolutions per minute
SLHX	suction line heat exchanger
TE	thermoelectric
TEC	thermoelectric cooler
VC	vapour compression

Symbols

A_s	surface area (m^2)
c_p	specific heat in constant pressure (kJ kg^{-1} °C^{-1})
D	depth of the compartment (mm)
d_F	fan diameter (mm)
g	acceleration due to gravity (9.81 m s^{-2})
h	convection heat transfer coefficient (W m^{-2} K^{-1})
H	height of the compartment (mm)
H_T	height of the TEC
I	electric current (A)
k	thermal conductivity (W m^{-1} °C^{-1})
L	length (m)
L_c	characteristic length (m)
m	mass (kg)
p	static pressure (Pa)
P_s	perimeter of the surface (m)
Q_C	cooling effect (W)
$Q_{C,TEC}$	thermoelectric cooler cooling effect (W)
Q_H	heating effect (W)
$Q_{H,TEC}$	thermoelectric cooler heating effect (W)
t	time (s)
T	temperature (K)
T_a	ambient temperature (K)
T_{cc}	target temperature of chill compartment (°C)
ΔT	temperature difference (°C)
V	velocity vector (m s^{-1})
∇	gradient operator
W	width of the compartment (mm)
W_T	width of the TEC (mm)
W_i	width of the TEC inlet (mm)
$W_{comp,in}$	compressor power (W)

Greek symbols

β	β is the coefficient of volume expansion (K^{-1})
ρ	air density (kg m^{-3})
μ	dynamic viscosity (Pa s)
ν	kinematic viscosity of the air (m^2 s^{-1})
Φ	viscous-dissipation function

exchangers. Vian and Astrain (2009b) introduced a domestic refrigerator, without moving parts, with only fresh food compartment cooled by TECs. To increase the rate of heat transfer, a thermosyphon with two-phase and capillary lift design was applied on the cold side of the TEC, whereas another thermosyphon, with two-phase and without fan was applied to the hot side of the TEC. The experimental results showed that the compressor-based refrigerator had half the electric power consumption of the TE refrigerator. Martinez et al. (2013) studied the influence of three different temperature control systems on the electric power consumption and COP of a TEC: (1) an on/off controller (2) a proportional–integral–derivative controller (3) a novel operating system based on idling voltages (IVs). Their study proved that the controller based on IVs decreases the electric power consumption of the refrigerator by 32% and increases the COP by 64%, compared with the on/off controller. Riffat et al. (2001) investigated the application of heat pipes and phase change materials for TE refrigeration. They constructed two different TE refrigerators: the first employed a conventional heat sink system (bonded fin heat sink) on the cold side of the TEC. The other had an encapsulated phase change material in place of the conventional heat sink. Both refrigerators employed heat pipe embedded fins as the heat sink on the hot side. In their study it was found that application of an encapsulated phase change material improved the performance of the TE refrigerator. Jugsujinda et al. (2011) investigated a TE refrigerator's performance. The study showed that TE refrigerator's maximum COP was 0.65 WW^{-1}. Min and Rowe (2006) developed prototype TE domestic refrigerators and they evaluated them regarding the COP, heat-pumping capacity and cooling-down rate. They found that the COP of TE refrigerator was around 0.3–0.5 WW^{-1} for the operating temperature of 5 °C with ambient temperature at 25 °C.

Modelling and numerical analysis have been developed and adopted for the TECs in different studies. The chief parameters marked mainly in those studies are *Seebeck*, *Peltier*, *Thomson* and *Joule* effects. Yamanashi (1996) analysed TEC's optimum design conditions in a system with heat exchangers. The aim was to achieve the best performance under a constant temperature difference and heat load. Heat balance equations were presented as well as dimensionless entropy flow equations, exergy flow and exergetic efficiency. He concluded that the hot side heat exchanger of the TEC has more considerable effect on degrading the overall TEC system than does the cold side heat exchanger. Fraisse et al. (2013) focused on TE leg and proposed to compare different simplified models with the more accurate ones. These models are standard and improved simplified, analytical, electrical analogy, and numerical models based on finite element method (FEM) software. Their study presented that the electrical analogy model, which gives almost the same results with FEM, is more efficient. Perez-Aparicio et al. (2012), combined FEM with Monte Carlo technique to simulate a commercial TE cell. Kim and Kim (2015) developed computer software to predict the *Seebeck* and *Peltier* effects for TE devices. A novel approach for optimisation of two-stage TE refrigeration systems using a chemical reaction optimisation (CRO) algorithm was proposed by Hadidi (2017).

The numerical simulation studies for household refrigerators through computational fluid dynamics (CFD) have drawn attention because the method successfully predicts the air temperature and velocity distribution in the compartment to be simulated. It is

critical to comprehend the air temperature and flow characteristics inside the compartments because it provides insight into the cooling performance of the refrigerator. Evenly distributed cooled air inside the compartment averts temperature stratification, that is, it prevents the formation of warmer regions which cause the deterioration of the perishable foodstuff (Yang et al., 2010; Belman-Flores and Gallegos-Muñoz, 2016; Belman-Flores et al., 2014). There are works conducting the comparison of various simulation tools, such as between CFD and Artificial Neural Network (ANN) (António and Afonso, 2011; Kumlutas et al., 2012; Avcı et al., 2016), between CFD and Proper Orthogonal Decomposition (POD) (Bayer et al., 2013). In these works, it is shown that the ANN and POD methods produced satisfactory results along with CFD.

The CFD method also provides insights about the heat leakages through the door gaskets of the refrigerators as presented by Gao et al. (2017). Researchers are interested in the impact of radiation on the cooling performance of household refrigerators by means of CFD; they indicated that the radiation affects air circulation, natural convection and heat transfer inside the refrigerators (Zhang and Lian, 2014; Laguerre et al., 2007; Laguerre et al., 2010a). Numerical and mathematical models have been developed and verified through the experimental tests for different types of household refrigerators under different conditions (Ledesma and Belman-Flores, 2017; Gupta et al., 2007; Amara et al., 2008; Laguerre et al., 2010b; Todorov et al., 2017; Fukuyo et al., 2003; Ding et al., 2004).

Limited simulation analysis has been performed on the refrigerators in which a TEC is installed. A computational model was developed and advanced to analyse the thermal and electric performance of a Peltier based thermoelectric refrigerator (Astrain et al., 2005; Martinez et al., 2016). This model's results were validated with the experimental test results and thus, it was proved that using TE cooling technology can be beneficial to household refrigerators.

This work provides numerical simulation (CFD) and experimental data of a household refrigerator including VC and TE cooling technologies. To the authors' knowledge, there has been no such work so far which (1) presents air temperature fields and flow distributions inside the refrigerator compartment cooled by TEC and (2) investigates TEC performance regarding the energy consumption and cooling down time rate in compliance with new IEC 62552:2015 standard (*Household refrigerating appliances – Characteristics and test methods*) (IEC-62552:2015, 2015).

1.2. Objectives of current work

This work follows on prior work by Soylemez et al. (2018). In the given work, two different hybrid refrigerators were built based on a serial Bosch KGN39 premium refrigerator. The experimental analysis was conducted to determine the cooling performance of hybrid refrigerators, particularly the impacts of the TEC on the system operation. According to the results obtained by Soylemez et al. (2018), the promising hybrid refrigerator, Hybrid II, which had superior performance results in terms of energy consumption and cooling capacity, was chosen for further improvements. In the aforecited study, the TEC was mounted on the door of the refrigerator in order to cool the fresh food compartment (FFC) as seen in Fig. 1. For the purpose of this study, this refrigerator is considered as reference and called Hybrid household refrigerator I (HHR I).

The primary purposes of this work are (1) to simulate the air temperature and velocity distribution inside the FFC by CFD analysis, validated with the test data of HHR I to locate the TEC at the most optimum position (2) to build new HHRs according to the simulation results and validate them by experimental analysis (3) to enhance overall performance of the HHR by additional improvement measures.

2. Methodology of the work

It will be very serviceable to employ a relevant methodology for the current study to reach its objectives. After setting the targets and conducting the literature survey for the similar experimental and numerical studies, the CFD tool was preferred for the simulation of HHR because it had already provided satisfying achievements regarding the visualisation of the temperature and flow fields inside the compartments. This enabled researchers to find optimum cooling performance values for their applications. Final configurations were determined and then it was aimed to verify numerical analysis by experimental analysis. Hence, two tests, energy consumption and cooling capacity, were performed complying with IEC62552:2015. This standard was opted for: (1) being a new standard; thus, there is no test data with it except former study of this work (2) easier execution of the tests: no packages are used (except warm packages used for cooling capacity tests) minimising inconsistency and uncertainty of the tests. Additional improvements were also implemented for further developments.

3. Experimental analysis

3.1. Properties of HHRs

The HHRs are based on a Bosch KGN39 premium refrigerator, a bottom freezer type with two doors and three compartments (see Fig. 1): *fresh food compartment (FFC) with a net volume of 175 l, chill compartment (CC) with a net volume of 81 l and freezer compartment (FC) with a net volume of 87 l*. The FFC of all HHRs is cooled by the TEC and the rest of the compartments are cooled by compressor-based VC system.

VC cooling system of HHRs has a single cooling circuit with a variable speed compressor, an air-cooled evaporator and two skin condensers in the side walls. The warm air is cooled in the evaporator and the freshly cooled air is circulated by a fan through air channels to the CC or FC (Soylemez et al., 2018).

The TEC, CTA305, is manufactured by Marlow with a capacity of 143 W. It was selected to match the heat load requirements of FFC. The heat load requirements' calculations are based on the measurements of overall transmission losses and the calculations stated in the former study (Soylemez et al., 2018).

3.2. Standards, specifications and tests

The energy consumption and cooling capacity tests were performed in conformity with the new IEC62552:2015 standard. It is a worldwide standard which was prepared by the committee representing government agencies, independent institutions and household refrigerator manufacturers from all over the world. The primary purpose of this standard is to develop a test method to reflect operating conditions and usage patterns of household refrigeration products in different climates and regions around the world. It also aims to measure the key components of energy consumption. These can be divided into two groups: (1) operating conditions: ambient temperature, temperature control setting, user interactions and appliance installation of (2) product design: defrost and recovery characteristics, defrost interval during normal use, load processing efficiency, the quality of thermal insulation, operation of certain auxiliaries and the dimensions of the product (IEC-62552:2015, 2015).

Because this new standard will replace the current standards, which only meet their regional requirements, it was con-

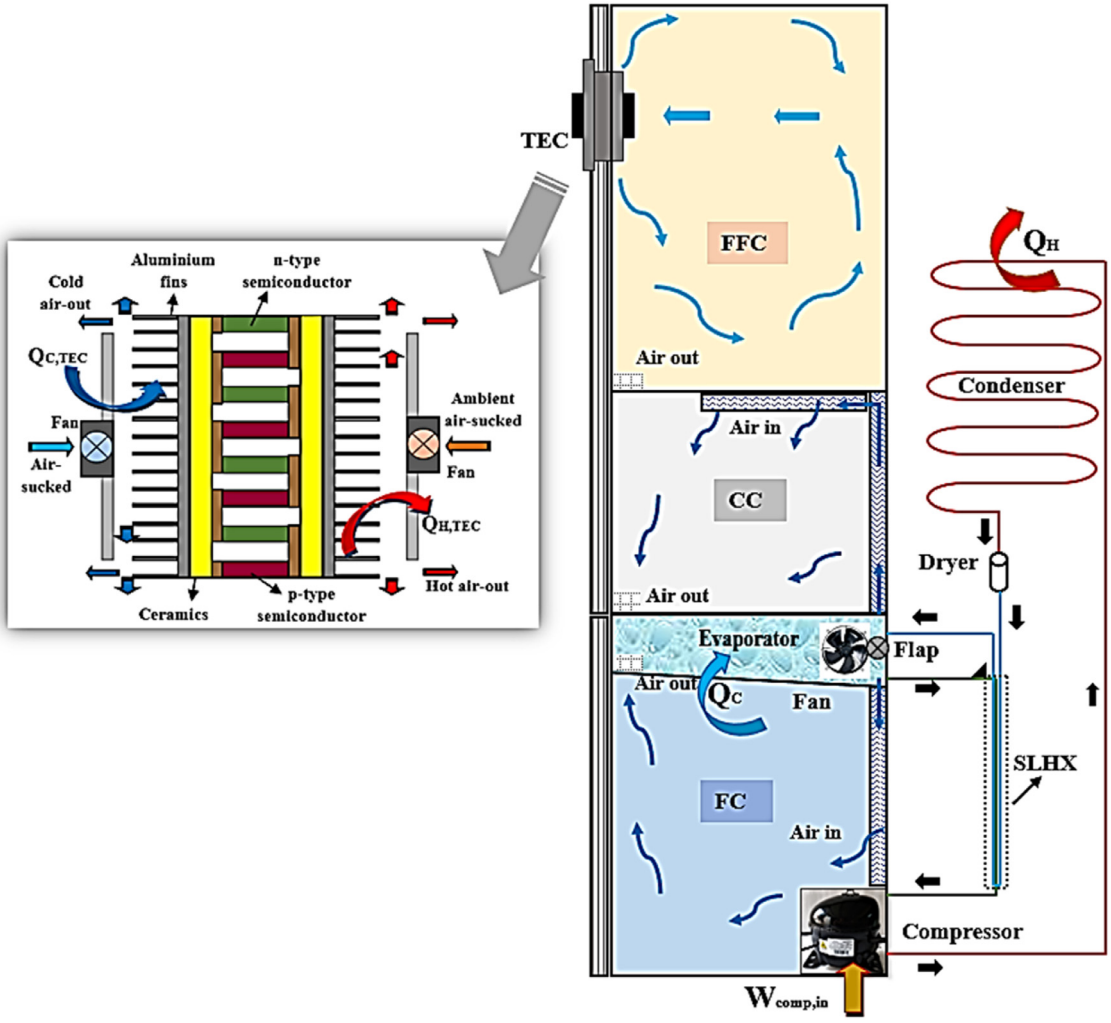

Fig. 1. HHR I.

Table 1
Compartment target temperatures and loading conditions for the tests.

Tests	Ambient	FFC		CC		FC	
	[°C]	Target temp. [°C]	Measured by	Target temp. [°C]	Measured by	Target temp. [°C]	Measured by
Energy consumption	16.0 ± 0.5 and 32.0 ± 0.5	≤+4.0	Cu cylinder	≤+2.0	Cu cylinder	≤−18.0	Cu cylinder
Cooling capacity	25.0 ± 0.5	≤+4.0	Cu cylinder Warm packages	$-3.0 \leq T_{cc} \leq +3.0$	Cu cylinder	≤−18.0	Cu cylinder

sidered as reference in this study. In Table 1, the target compartment temperatures and loading conditions for the tests are given.

Energy consumption test is performed at two different ambient temperatures of 16 °C and 32 °C with different temperature control settings. The results at each setting are interpolated to target compartment temperatures to estimate energy consumption at each ambient temperature.

In terms of cooling capacity test, the refrigerator is prepared as for the energy consumption test. The temperature transducers inside the compartments have exactly the same locations with the ones in energy consumption test. However, the test is conducted at an ambient temperature of 25 °C. After the target compartment temperatures meet the requirements and reach the steady state conditions, the warm packages are introduced into the FFC.

Temperature transducers used for the measurements are inserted into the M-packages of warm packages used in cooling capacity test or into the centre of Cu cylinders which are solid masses made of brass or tin-covered copper having masses of 25 g ±5%.

3.3. Climate chambers

The climate chambers were located at the R&D Cooling Centre of BSH Bosch Household Appliances in Çerkezköy, Tekirdağ, Turkey. The humidity and temperature inside the chambers can be set as required. The humidity was kept between 35% and 50% during the

tests. The temperature inside the chamber ranges between 10 °C and 43 °C.

It is possible to collect temperature, pressure, mass flow and power test data at each test station inside the chambers. Test data were collected by means of data acquisitions and then transmitted to the BSH test software to analyse the results.

3.4. Measurement instruments

Quality instruments with high accuracies were used in the experiments. Power was measured with an accuracy of 0.025% by a Zimmer LMG500 power meter and energy consumption were measured with an uncertainty of less than 2%. Relative humidity had an overall uncertainty of measurement not greater than 5%. Calculated values of test duration, made up of the difference between times recorded at each sampling period, had an expanded uncertainty of 0.1%. T type calibrated thermocouples were used as temperature instruments with a measurement uncertainty of ±0.2 °C. The test data were collected by the datalogger, an Agilent 34970A.

For cooling test, the packages which consist of oxyethylmethylcellulose, sodium chloride and water, described in the given standard (IEC-62552:2015, 2015), were used. Dimension tolerances for the packages were ±2 mm for small packages, ±3 mm for larger ones. The tolerances of masses of the packages were ±2%.

To measure the air velocities inside the FFC a Testo 425, thermal anemometer was used. It is well suited to low air flow velocity (0–20 m s^{-1}) with an accuracy of ±0.5 °C and resolution of 0.01 m s^{-1}.

4. Numerical analysis

The main goal of numerical analysis in the context of this study is to gain an idea about the air temperature and flow field inside the FFC in order to place the TEC at the most optimum position. Since the focus in the study is to improve the HHR, a simpler and less time-consuming way of simulation was considered to be satisfactory.

Reference test data were collected from HHR I's FFC when the room temperature and temperature inside the FFC were around 25 °C and 4 °C, respectively. ANSYS R18.1 FLUENT was used in the numeric analyses. Five different configurations were analysed to find the optimum location for the TEC. For CFD analysis, the following assumptions were made:

- The fluid flow is incompressible because of a low Mach (Ma) number, $Ma < 0.3$.
- The flow is assumed as steady state.
- The analysed compartment, FFC, is unloaded.
- Air leakages through the gaskets are neglected.
- Boussinesq model is considered.
- Radiation effects are neglected.
- Flow inside the FFC is turbulent
- Forced convection occurs inside the FFC.

4.1. Mathematical model/governing equations

The model is developed considering the above assumptions; it consists of three key governing equations, Eqs. (1)–(3).

4.1.1. Conservation of mass (continuity equation)

For incompressible flow, the equation for conservation of mass, also called the continuity equation, is demonstrated in Eq. (1)

$$\nabla \cdot \vec{V} = 0 \tag{1}$$

where $\vec{V}$ is fluid velocity and ∇ is the gradient operator.

Table 2
Details for the meshing.

Parameters	Values
Sizing	
Size function	Curvature
Relevance centre	Fine
Transition	Slow
Span angle centre	Fine
Curvature normal angle	18°
Min size [m]	0.00009
Max face size [m]	0.0047585
Max tet size [m]	0.5
Quality	
Smoothing	Medium
Statistics	
Nodes	673,347
Elements	3501,386

4.1.2. Conservation of momentum (Navier–Stokes equations)

For incompressible flow of Newtonian fluids, the conservation of linear momentum is governed by the Navier–Stokes equation.

$$\rho \frac{D\vec{V}}{Dt} = \rho\vec{g} - \nabla p + \mu \nabla^2 \vec{V} \tag{2}$$

Here, ρ is the fluid density, $\vec{g}$ is gravitational acceleration, p is the static pressure, μ is the dynamic viscosity coefficient. In Eq. (2), D/Dt represents the material (or substantial) derivative, and $\nabla^2$is the Laplacian operator.

4.1.3. Conservation of energy

The first law of Thermodynamics written for the incompressible air in the FFC is given in following equation:

$$\rho c_p \frac{DT}{Dt} = k\nabla^2 T + \Phi \tag{3}$$

where, c_p is the heat capacity under constant pressure, T is the fluid temperature, k is the thermal conductivity of the fluid and Φ is the dissipation function.

4.2. Geometric model

Because the real geometry of the FFC has many complexities, the geometric model was simplified to provide the most optimum mesh size. In this way, the solution time was significantly decreased. The model was geometrically symmetric and drawn by means of the Solidworks software and then transferred to the ANSYS DesignModeler to prepare for meshing. The simplified geometries of the FFC and the TEC are demonstrated in Fig. 2.

The dimensions are 695 × 495 × 515 mm for FFC's $H \times W \times D$ and 150 × 250 × 30 mm for $H_T \times W_T \times W_i$ of the TEC's cold face. The diameter of the TEC's fan (d_F) is 120 mm.

4.2.1. Meshing the geometry

The geometry of FFC was meshed using ANSYS AUTODYN. The details of the mesh for HHR I's FFC geometry (including TEC) are given in Table 2. An unstructured mesh composed of tetrahedron (tet) elements was constructed.

4.2.2. Convergence of solution and mesh independent study

In this section, the aim is to quantify mesh accuracy by presenting different mesh quality parameters such as element quality value and distribution, skewness and aspect ratio and warping factor. Their distributions are presented in Fig. 3.

The skewness ratio is the most important meshing quality parameter. Its average value must be between 0 and 1. If it is be-

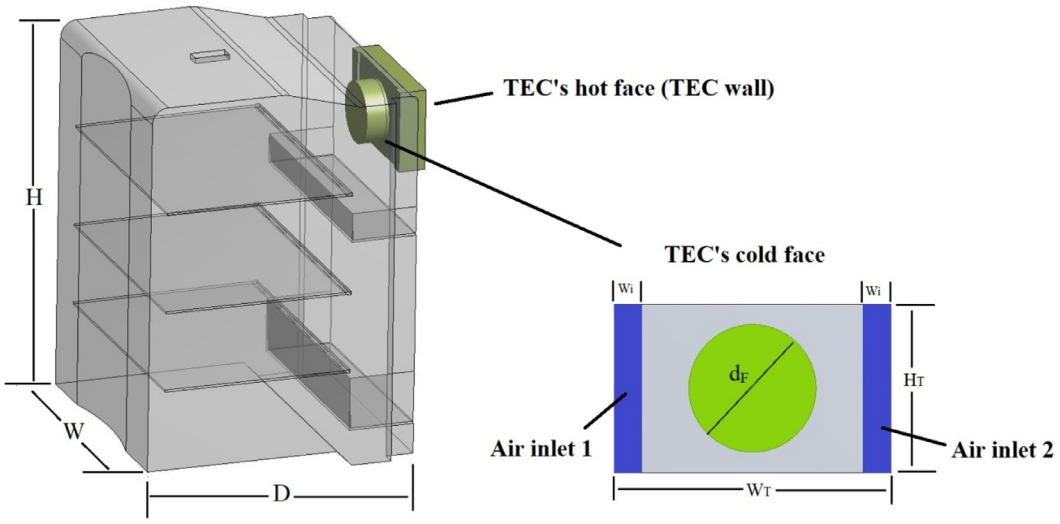

Fig. 2. Geometric model of the FFC and TEC.

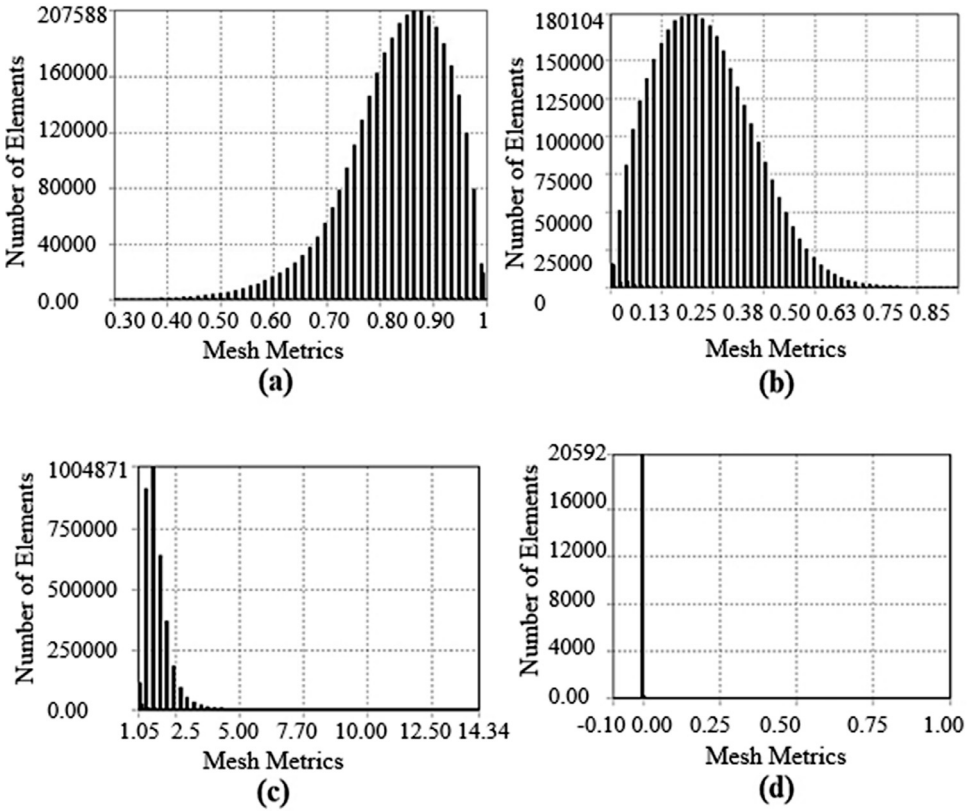

Fig. 3. (a) Element quality value and distribution, (b) skewness ratio, (c) aspect ratio, (d) warping factor.

Table 3
Material properties.

Quality	Value	Reference value	Result
Element quality	0.836	0–1	Optimal
Skewness ratio	0.228	0–1	Excellent
Aspect ratio	1.849	1–∞	High quality
Warping factor	4.70E–15	0–1	High quality

tween 0 –0.25, the meshing quality is 'Excellent'; between 0.25–0.50, it is 'Very Good'; between 0.5–0.80, it is referred as 'Good'. The ideal value for aspect ratio is 1 and for warping factor is 0. The average value of element quality must also be between 0 and 1. The ideal value for it is 1. In Table 3, the average values for quality meshing parameters are summarised.

In order to perform a mesh independence study, variations of inner wall surface temperatures at 14 different locations (see Fig. 4) of the FFC with respect to the mesh size were monitored. For this purpose, initial solutions were obtained for a mesh size of 500,000 cells, then the mesh size was gradually increased to 5000,000 cells. Here, only the minimum cell size and the maximum face size were changed, while other mesh parameters were kept constant. For each mesh size, the residual for continuity, momentum and energy equations were monitored as well as inner wall surface temperatures. The variations of wall temperatures with respect to the mesh size are demonstrated in Fig. 5.

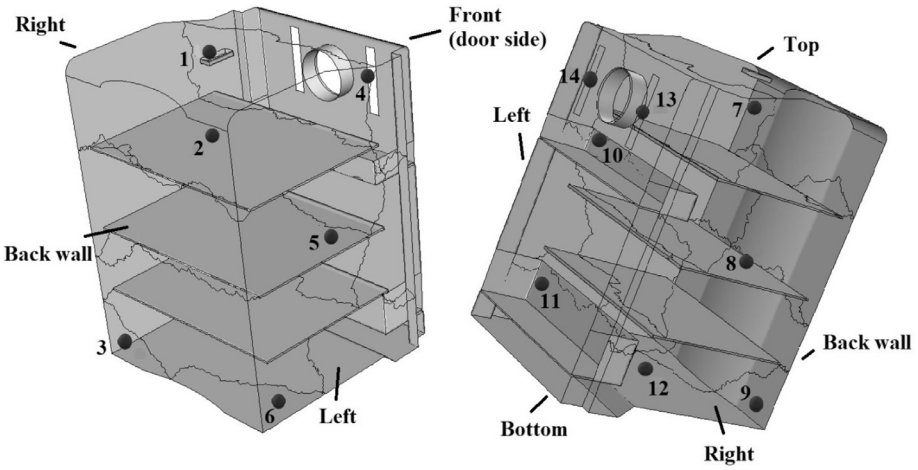

Fig. 4. The location of surface temperatures.

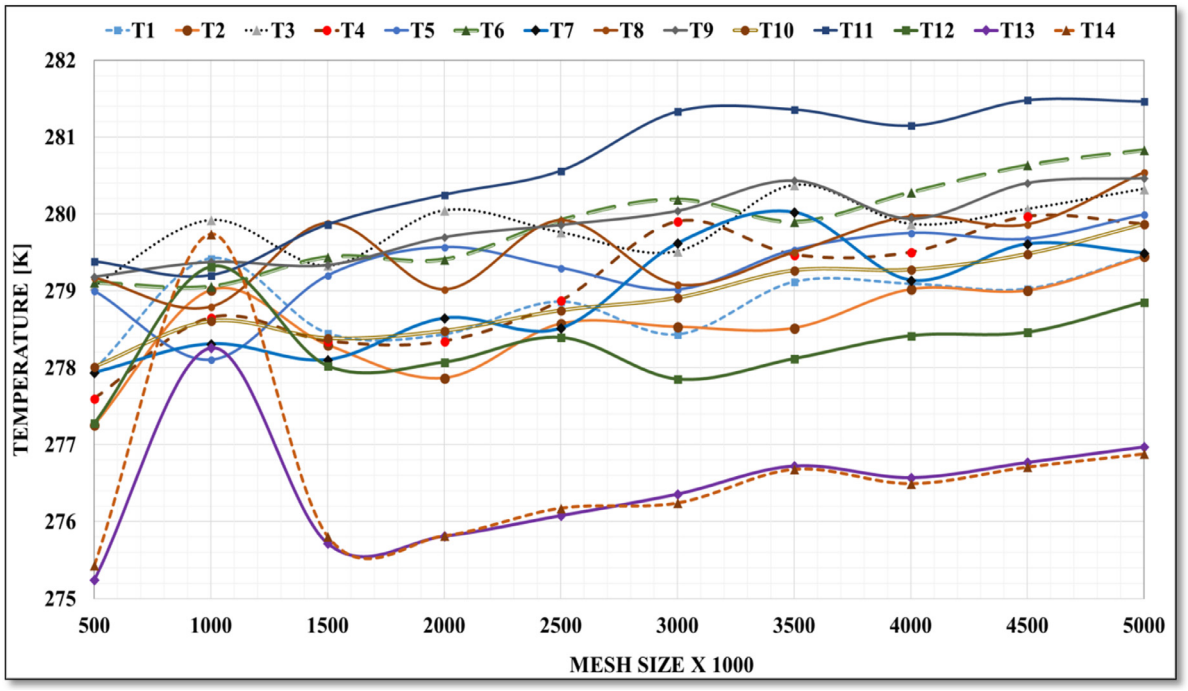

Fig. 5. Determination of mesh size.

According to Fig. 5, the temperature predictions did not exactly become mesh independent. However, considering the scale of the vertical axis of Fig. 5 and noting the fact that the main purpose of the CFD predictions here is to rank different configurations in terms of velocity and temperature distributions, the average temperature variation after the mesh size of 3500,000 is assumed to be small enough. Therefore, mesh size of 3500,000 is used in the rest of the study; analysis by Belman-Flores et al. (2014) determined that a similar mesh size could be applied to an FFC.

4.3. Numerical model

A viscous model of realisable k-epsilon model with a standard wall function was applied. As options, full buoyancy effects and curvature correction were considered. Regarding the solution methods, SIMPLE algorithm, with second order upwind discretisation for pressure, momentum, and turbulent kinetic energy and first order upwind discretisation for turbulent dissipation rate were used. The maximum number of iterations was 7500 in each solution.

4.4. Properties of materials

The properties of the materials are summarised in Table 4.

4.5. Boundary conditions

The boundary locations of FFC are shown in Figs. 2 and 4. The boundary conditions are also presented in Table 5. For the thermal boundary conditions, the real average surface and ambient temperature measurements on the FFC were considered. The ambient temperature was 25.05 °C (298.20 K). Yet, around the hot face of the TEC (TEC wall) and on the side walls of FFC (due to the skin condensers) the surface temperatures were relatively higher. For the bottom wall's surface and ambient temperature values, the temperature measurements inside the CC were regarded.

Table 4
Material properties.

Materials	ρ [kg m^{-3}]	C_p [J kg^{-1} K^{-1}]	k [W m^{-1} K^{-1}]
Fluid			
Air	1.225	1006.43	0.0242
Solid			
Aluminium	2719	871	202.4
Expandable polystyrene	26.25	1200	0.0345
Polyurethane	34.5	1500	0.022
Vacuum insulated panel	225	1050	0.005

Table 5
Boundary conditions for the FFC.

Boundary	Thermal conditions	Ta [K]	h [W m^{-2} K^{-1}]	v [m s^{-1}]
Air inlet				
Inlet 1	–	274.4	–	2.10
Inlet 2	–	274.6	–	2.45
Air outlet				
Walls				
Top wall	Convective	298.2	1.80	No slip
Side walls	Convective	305.7	2.91	No slip
Front wall	Convective	298.2	1.64	No slip
Back wall	Convective	298.2	2.15	No slip
Bottom wall	Convective	275.7	2.17	No slip
TEC				
TEC wall	Convective	300.1	16.37	No slip

The model was geometrically symmetric however the boundary conditions for the air inlets were not, because the data for them were collected from the measurements. In consequence, the inlet temperatures are almost identical and there is a difference in the air velocities by around 15%.

The heat was removed by the skin condensers located in the side walls and there was no fan, thus the main heat transfer mechanism was natural convection. However, there was a fan on the hot side of the TEC and therefore for the TEC wall, forced convection was considered. The empirical correlations used for the walls to calculate convective heat coefficients (h) are (Çengel, 2006):

$$h = \frac{N_U k}{L_c} \tag{4}$$

In where, N_u is Nusselt number, k is the thermal conductivity and L_c is the characteristic length. The values for k was collected from the tests to measure overall transmission losses of the compartments as stated in Soylemez et al. (2018). The equations for N_u are:

For side walls, rear and front wall (case of vertical plate):

$$N_u = \left\{ 0.825 + \frac{0.387 {Ra_L}^{1/6}}{[1 + (0.492/\mathrm{Pr})^{9/16}]^{8/27}} \right\}^2 \tag{5}$$

For the top wall (case of horizontal plate):

$$N_u = 0.54 {Ra_L}^{1/4} \tag{6}$$

For the bottom wall (case of horizontal plate):

$$N_u = 0.27 {Ra_L}^{1/4} \tag{7}$$

In Eqs. (5)–(7), Ra_L is the Rayleigh number, which is the product of the Grashof (Gr_L) and

Prandtl (Pr) numbers. Its formula is given as follows:

$$Ra_L = Gr_L \mathrm{Pr} = \frac{g\beta(T_s - T_\infty){L_c}^3}{\nu^2} \mathrm{Pr} \tag{8}$$

Table 6
Surface temperatures.

Temperatures	Test [K]	CFD [K]	Δavg [K]
T1	278.2	279.1	0.9
T2	277.8	278.5	0.7
T3	279.3	280.4	1.1
T4	277.9	279.5	1.6
T5	278.2	279.5	1.3
T6	279.1	279.9	0.8
T7	277.5	280.0	2.5
T8	279.1	279.5	0.4
T9	279.1	280.4	1.3
T10	278.4	279.3	0.9
T11	279.8	281.4	1.6
T12	277.2	278.1	0.9
T13	277.9	276.7	−1.2
T14	278.2	276.7	−1.5

where β is the coefficient of volume expansion (K^{-1}) and ν is the kinematic viscosity of the air (m^2 s^{-1}). L_c was the height of the FFC for the side, rear and front walls. For the top and bottom ones, it was

$$L_c = \frac{A_s}{p_s} \tag{9}$$

where A_s and P_s are the surface area and perimeter, respectively.

5. Results

5.1. CFD results

Five different configurations were created and then simulated with the same solution method and mesh size of around 3500,000. In each configuration, the TEC was placed at a different location.

5.1.1. Reference CFD analysis

As mentioned in Section 4.2.2, the inner wall surface temperatures of FFC (HHR I's FFC), including TEC's cold face, were measured from 14 different points as shown in Fig. 4. To validate the CFD predictions, numerical and experimental results were compared for these temperatures.

Table 6 shows the comparison of temperature predictions at the 14 locations shown in Fig. 5 with the corresponding measurements. Overall, there is a good agreement between the CFD predictions and experimental results.

The air streamlines and temperature distribution inside the FFC are demonstrated in Fig. 6. Strong and intense streamlines can be observed in the upper regions, especially in the top part of the compartment which accounts for colder temperature values in this part.

The lower parts of the compartment are relatively warmer which is likely due to the TEC location. The slightly lower temperature region observed at the bottom is due to the location of the lowermost shelf (compartment floor) just above the chill compartment. The regions with the highest temperature values are the door side, between door shelves, and middle bottom of back wall. These results are reasonable because (1) the FFC door is thinner and has less insulation material (polyurethane) compared to the other walls (2) there is an air channel on the middle of back wall that decreases the insulation thickness by 20 mm.

To decrease temperature stratification and therefore, provide more uniform temperature and air flow distribution, the TEC can be located to a more suitable position. For this reason, five different configurations for FFC were proposed.

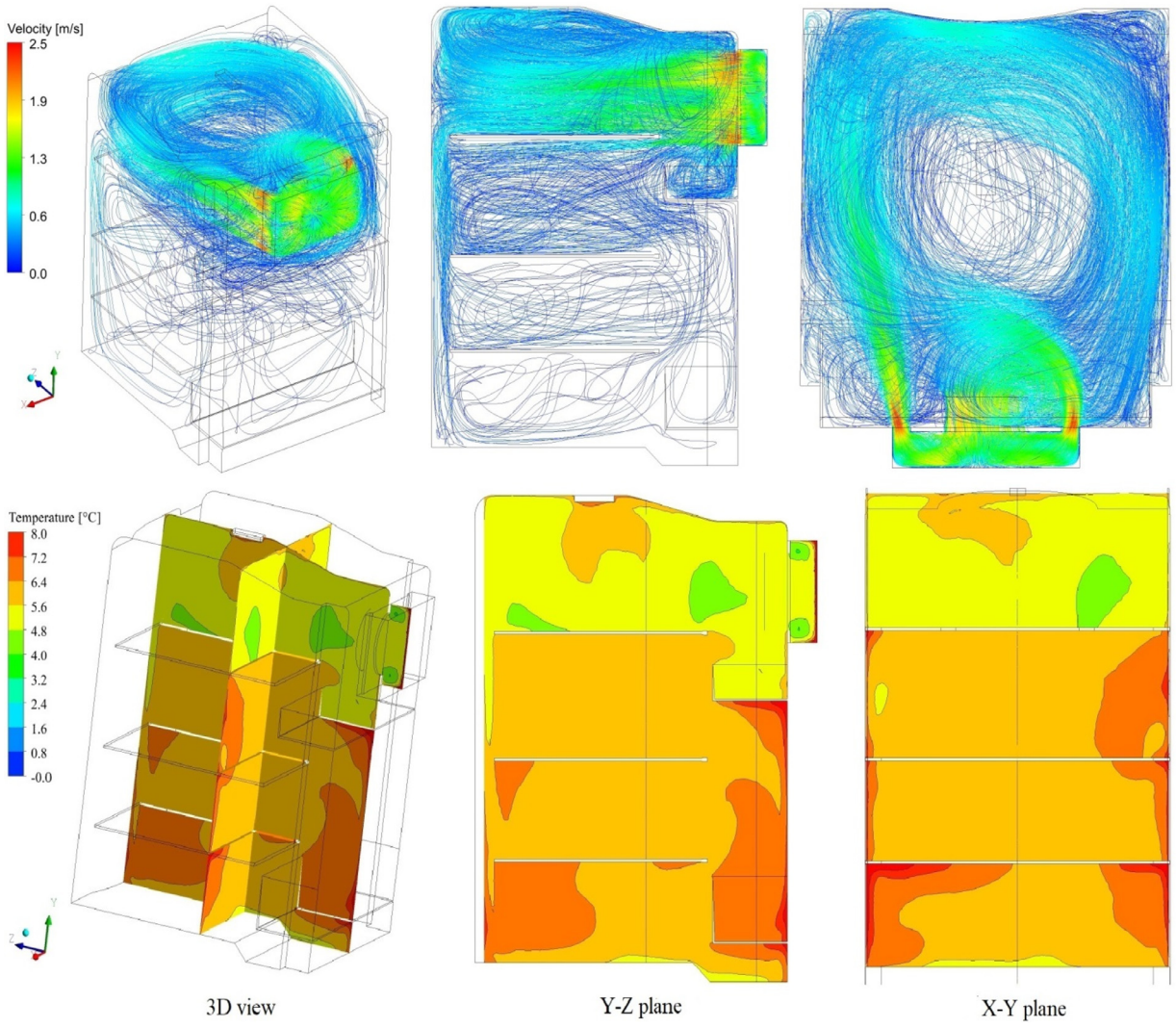

Fig. 6. Air streamlines and temperature distribution inside the FFC.

5.1.2. CFD analysis of proposed geometries

The CFD results can be seen in the figures below from Figs. 7–11.

- *Configuration 1*

In this configuration, the TEC is placed on the roof of the compartment.

- *Configuration 2*

The TEC is located at the top of the back wall of the compartment.

- *Configuration 3*

The TEC is placed in the middle of the rear wall of the compartment, between the top and middle shelves.

- *Configuration 4*

The TEC is horizontally positioned in the middle of the rear wall of the compartment and vertical to the top shelf. The cooled air is circulated through top and middle region of the compartment.

- *Configuration 5*

This configuration is like Configuration 4. However, the TEC has a vertical position rather than a horizontal positioning. The goal of this positioning is to circulate more cold air in the bottom region of the compartment.

In Configurations 1 and 2, it is obvious that the cooled air is trapped in the upper region of the compartment (between the top shelf and ceiling). For this reason, the upper region has the lowest temperature levels. The warmest zones are observed below the top shelf, particularly on the inner wall of the door between the door shelves and on the side walls just under the middle and bottom shelves.

Configuration 3 has a slightly better air flow and temperature field compared to Configurations 1 and 2. The cooled air is first circulated in the zone between the upper and middle shelves. The coldest region is the middle region, between the upper and bottom shelves. Although warmer areas on the door side are eliminated in this configuration, elevated temperature levels are observed in the upper region, especially in the zones just under the ceiling.

The location of the TEC in Configuration 4 and 5 leads to more uniform temperature distribution compared to other configurations. The temperature stratifications are almost eliminated. There are few small zones with relatively higher temperature values. Due

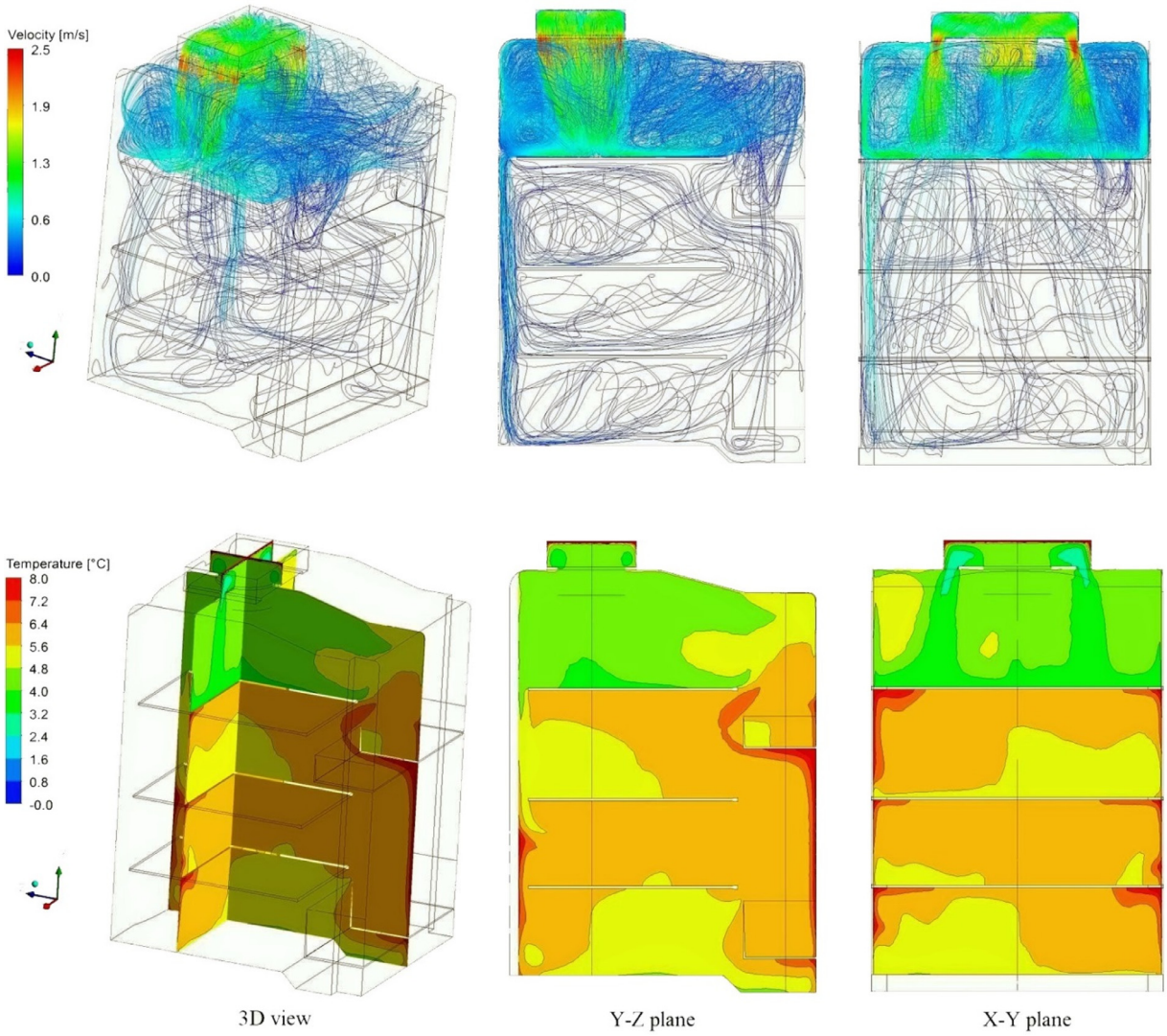

Fig. 7. Air streamlines and temperature distribution for Configuration 1.

to this, the previously mentioned HHR II and III were constructed based on Configurations 4 and 5, respectively.

5.2. Experimental analysis for HHR II and III

This section contains the energy consumption and cooling capacity test results obtained for HHR II and III. As mentioned earlier, these tests were performed in accordance with IEC62552:2015.

5.2.1. Energy consumption

An optimisation study was first conducted by analysing the effect of pre-specified improvement measures. Afterward, with the final configurations, the energy consumption and cooling capacity tests were performed.

5.2.1.1. Optimisation study. Measures for the enhancement of energy efficiency were applied to the HHR II and the final configurations, which give the highest energy efficiency, were fixed. The same configurations were also used for HHR III. The hysteresis for the TEC's temperature sensor inside the FFC (TEC hysteresis), the main and idling voltages (IVs) supplied to the TEC and compressor speeds were optimised in the given order. During the measurements for optimisation, only the steady state period of energy consumption test was analysed (defrost and recovery period was neglected) to save testing time. Yet, the energy consumption tests were fully performed with the final fixed configurations.

In the previous study (Soylemez et al., 2018), HHR I's TEC temperature hysteresis was adjusted regarding the cut-in and cut-off temperatures of the reference (series) KGN39P. In the FFC of this commercial refrigerator, the differences in the minimum and maximum air temperatures ranged from 1 °C to 4 °C. To keep the same temperature ranges and consume less energy, HHR I's TEC temperature hysteresis was fixed at 0.5 °C.

In this study, it became possible to set the temperature hysteresis of HHR II and HHR III to 1.1 °C and 2 °C, respectively. The hysteresis was increased thanks to more uniform air flow and temperature fields observed inside their FFC.

Following the hysteresis adjustment, the voltage of TECs' main supply for HHR II was optimised at an ambient temperature of 16 °C. The nominal voltage of the TEC main supply was 24 V; voltages of 20 V and 16 V were also supplied to the TEC. The results are presented in Table 7. For all the cases, the compartment temperature was 4.4 °C. The energy consumption was 0.916 kW h d^{-1} at nominal voltage; the lowest value was achieved at a voltage of 20 V with a value of 0.840 kW h d^{-1}. The energy consumption dropped by 8.3% due to the 12.2% increase in the TEC's COP. The TEC's COP

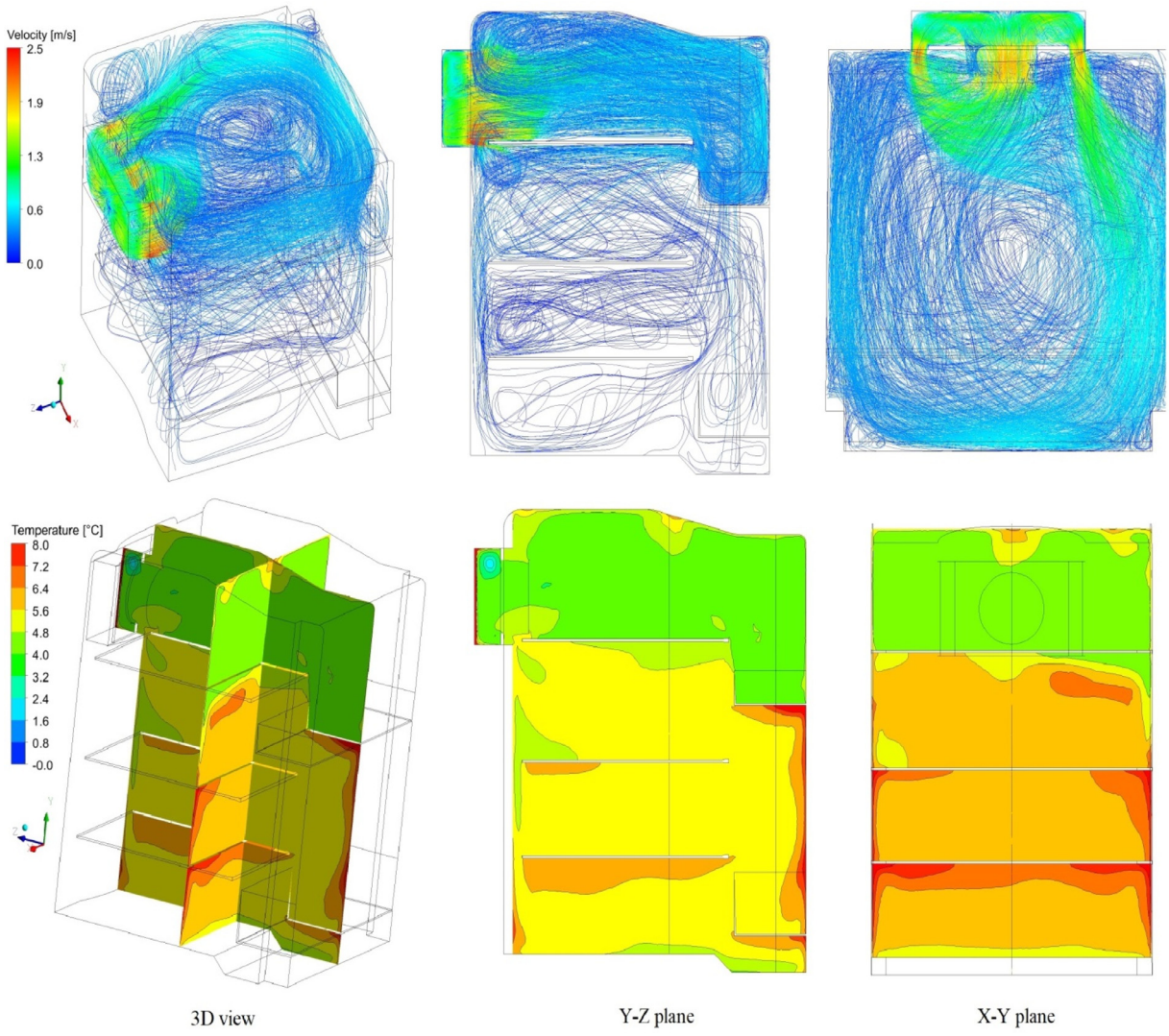

Fig. 8. Air streamlines and temperature distribution for Configuration 2.

Table 7
TEC main voltage optimisation for HHR II at 16 °C.

Main supply [V]	FFC temperature [°C]	Energy consumption [kW h d^{-1}]
16.0	4.4	1.070
20.0	4.4	0.840
24.0	4.4	0.916

Table 8
Applying idling voltages to HHR II at 16 °C.

IV [V]	FFC temperature [°C]	Energy consumption [kW h d^{-1}]
0.0	4.4	0.840
3.5	4.5	0.648
5.0	4.4	0.718

was 0.41 WW^{-1} and 0.46 WW^{-1} for the voltages of 24 V and 20 V, respectively. At 16 V, the highest energy consumption was seen due to the sharp increase in the TEC run time. Therefore, the main supply was set to 20 V.

Placing the TEC in the wall of the cabinet leads to an increase in heat transfer from ambient to the inside of the cabinet and therefore reduces the insulation quality. If the TEC has on/off operation cycle, the heat flow through the TEC is high during the off period. In the previous study (Soylemez et al., 2018), it was proved that the overall transmission losses rose by around 10% when the TEC was off. To avoid heat flow through the TEC, one of the solutions is to supply IVs to the TEC through the off period. That is to say, the TEC will have a continuous operation. The purpose is to keep the temperatures of the TEC's faces as close as the temperature of the environments they are in. The idea was originally proposed by Martinez et al. (2013).

In Table 8, the effect of supplied IVs to the HHR II's TEC on the energy consumption at 16 °C are presented. Here, the lowest energy consumption occurred with an IV of 3.5 V, 0.648 kW h d^{-1} which is 23% lower compared to the no IV case (0.840 kW h d^{-1}). Further increases in the IV have a negative effect on the energy consumption.

The detailed information about the effect of IVs on the TEC COP and energy consumption is given in Table 9. In this table, the analysis is based on a steady state period of approximately 6 h. The temperature of the TEC cold and hot faces and the upper region of the FFC are demonstrated. The temperature sensor location placed in the upper region of the FFC is shown in Fig. 12.

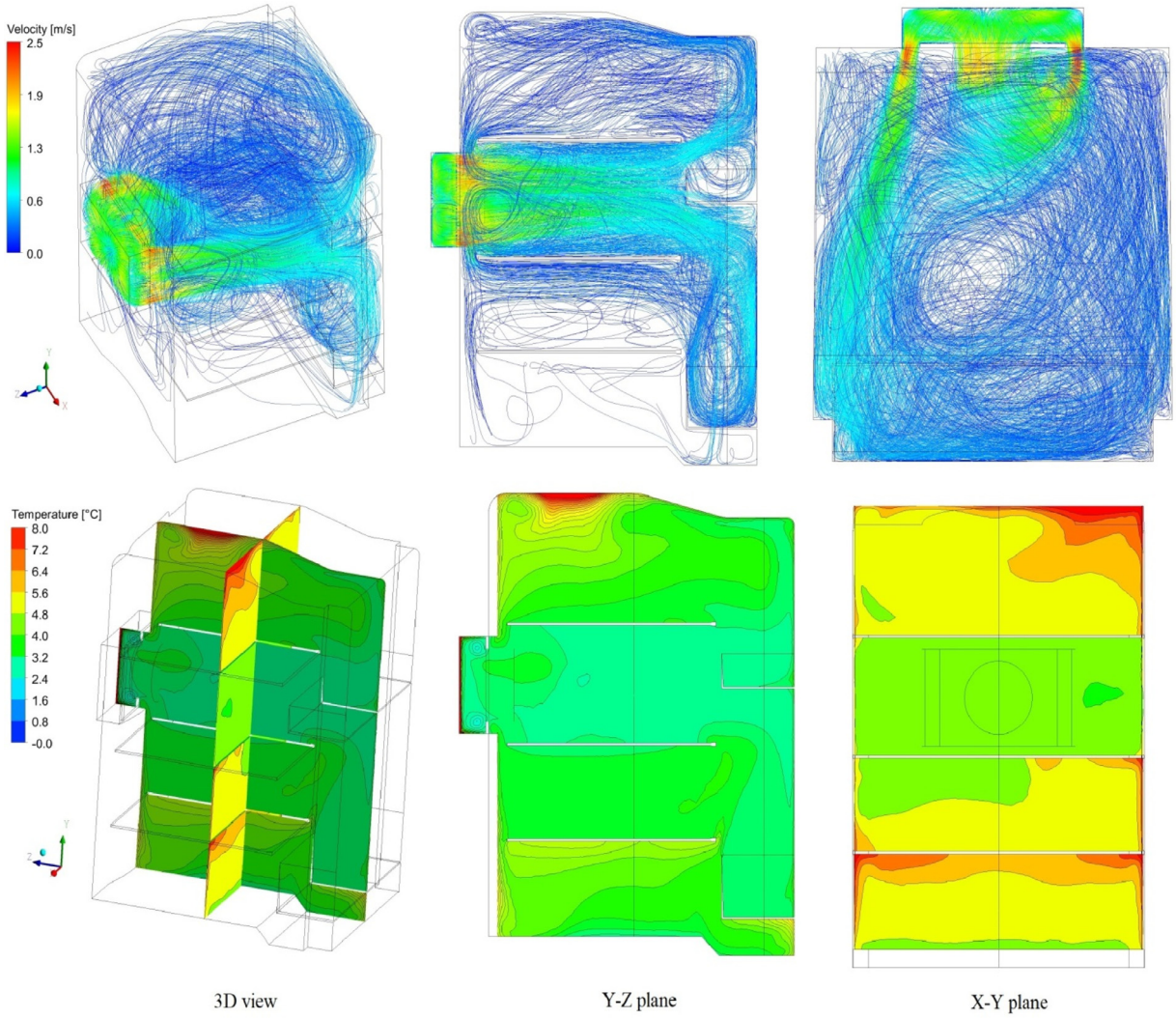

Fig. 9. Air streamlines and temperature distribution for Configuration 3.

Table 9
Effect of IVs on the COP of HHR II's TEC.

IV [V]	T_a [°C]	$T_{TEC\text{-}cold,min}$ [°C]	$T_{TEC\text{-}cold,max}$ [°C]	$T_{TEC\text{-}hot,min}$ [°C]	$T_{TEC\text{-}hot,max}$ [°C]	$T_{FFC\text{-}upper,min}$ [°C]	$T_{FFC\text{-}upper,avg}$ [°C]	$T_{FFC\text{-}upper,max}$ [°C]	$COP_{TEC,on}$ [WW^{-1}]	$COP_{TEC,idling}$ [WW^{-1}]
0.0	15.9	−2.2	11.6	11.4	21.7	2.7	4.6	6.6	0.46	–
3.5	15.9	−2.2	7.1	15.3	21.7	2.5	4.3	6.2	0.52	2.71
5.0	15.9	−2.5	6.8	17.6	21.7	2.4	4.2	6.1	0.52	2.05

In Table 9 and Fig. 12, the aim is to present temperature changes during the period of analysis to well understand the root causes of COP differences.

It is clear from Table 8 that with the IVs of 3.5 V and 5.0 V when the TEC is on (on period), the TEC's COP is higher than the without IV case by 13%. While supplying the IV to the TEC (off period), the TEC's COP is highest at 3.5 V with a COP value of 2.71 WW^{-1}. This explains the root cause of less energy consumption with supplying 3.5 V. To determine the optimum IV and therefore the highest efficiency during the off period, one should carefully analyse the temperature changes of the TEC's cold and hot faces. When supplying IV to the TEC, the aim should be to keep the TEC's hot face's minimum temperature as close to the ambient temperature (T_a) as possible while keeping the TEC's cold face maximum temperature at the same level of compartment temperature surrounding the TEC's cold face (in our case, the upper region of the FFC). Additionally, the minimum temperature of the TEC's hot face ought not to exceed the ambient temperature.

The same measurements for determining the optimum IV were also conducted at an ambient temperature of 32 °C. The ideal value of IV to be supplied to the TEC was 8.0 V as demonstrated in Table 10. The energy consumption was decreased by nearly 27% compared to the consumption of no IV case.

Although the primary focus of this study is to investigate the effect of the TEC on the household refrigerator's performance, an additional improvement step for optimising compressor speed at

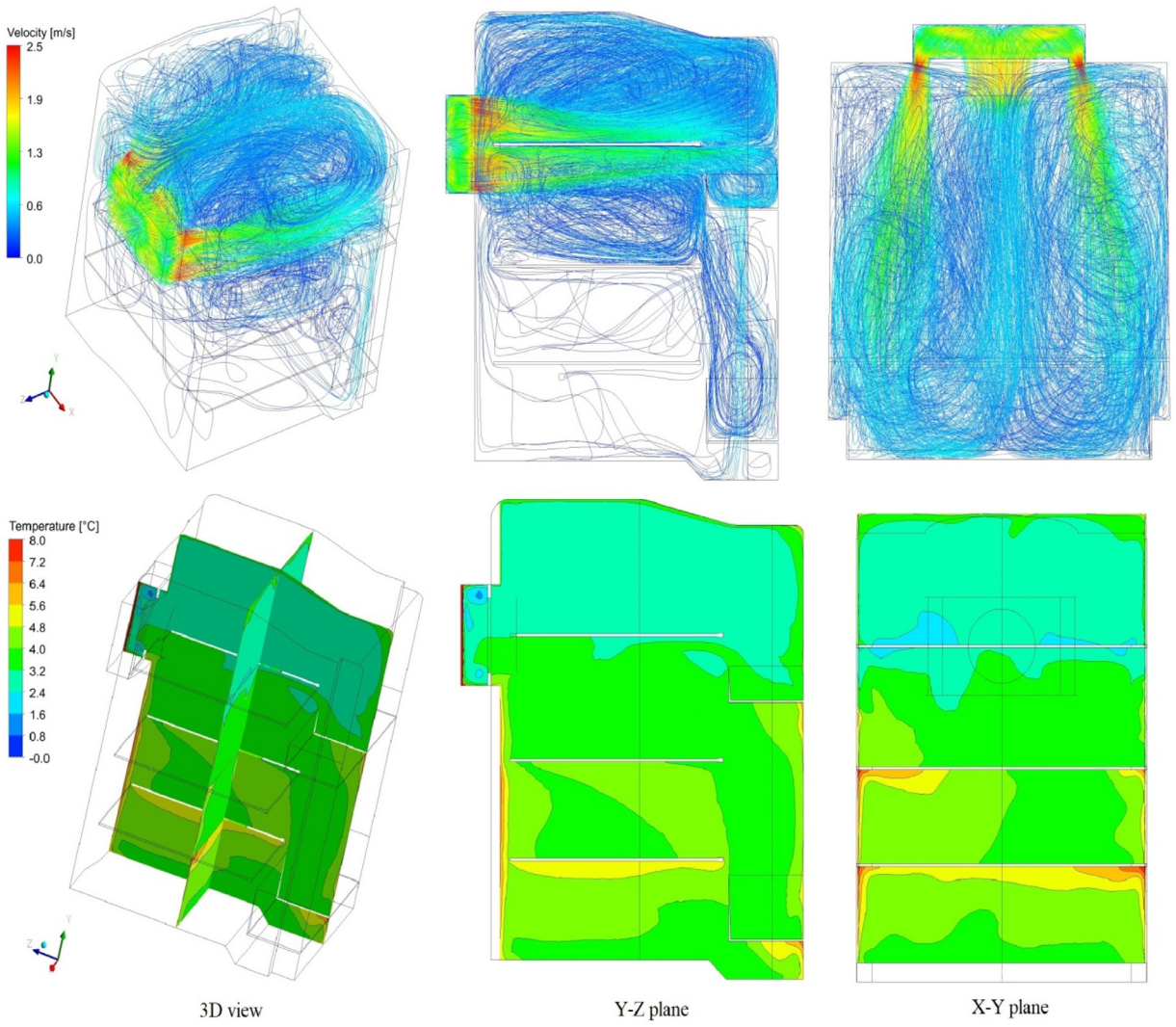

Fig. 10. Air streamlines and temperature distribution for Configuration 4.

Table 10
Applying idling voltages to HHR II at 32 °C.

Idling voltage [V]	FFC temperature [°C]	Energy consumption [kW h d^{-1}]
0.0	4.0	3.097
3.5	4.0	2.786
5.0	3.9	2.735
6.5	3.9	2.702
8.0	3.9	2.273

32 °C was also conducted. The variable speed compressors used for household refrigerators generally have speed ranges between 1000 rpm and 4500 rpm. At lower room temperatures, the compressor should run at relatively lower speeds due to reduced cooling load. Because HHR's compressors operate at optimum speeds at 16 °C room temperature, the optimisation was conducted at only 32 °C in this study. The compressor speed was decreased by 400 rpm which reduced energy consumption by 2% from 2.273 kW h d^{-1} to 2.224 kW h d^{-1}.

5.2.1.2. Energy consumption test. After improvement studies of HHR II and III were completed, the energy consumption tests were performed with their final configurations. The test results are presented in Table 11. At 16 °C room temperature, all HHRs have the same compressor speeds, whereas HHR II and III have 400 rpm less speed compared to HHR I at 32 °C (the exact compressor speeds are not mentioned due to privacy policy of BSH Bosch). According to the results, it can be remarked that HHR II and HHR III have almost identical energy consumption levels. The differences in their energy consumptions at 16 °C and 32 °C are 0.7% and 1.5%, respectively. Energy efficiency improvements of up to 10% and 27% were achieved at the ambient temperatures of 16 °C and 32 °C, respectively, compared to HHR I.

5.2.2. Cooling capacity

In the standard (IEC-62552:2015, 2015), this test is named as the "cooling capacity test". The reason for that is after measuring the time for the cooling of warm packages from 25 °C to 10 °C, load mass is calculated in kg. For the purpose of this study, only the cooling time was measured during the tests because this will provide an adequate idea about the performances of the HHRs.

Before performing the test, the HHRs were prepared and the temperature sensors were located as previously for the energy con-

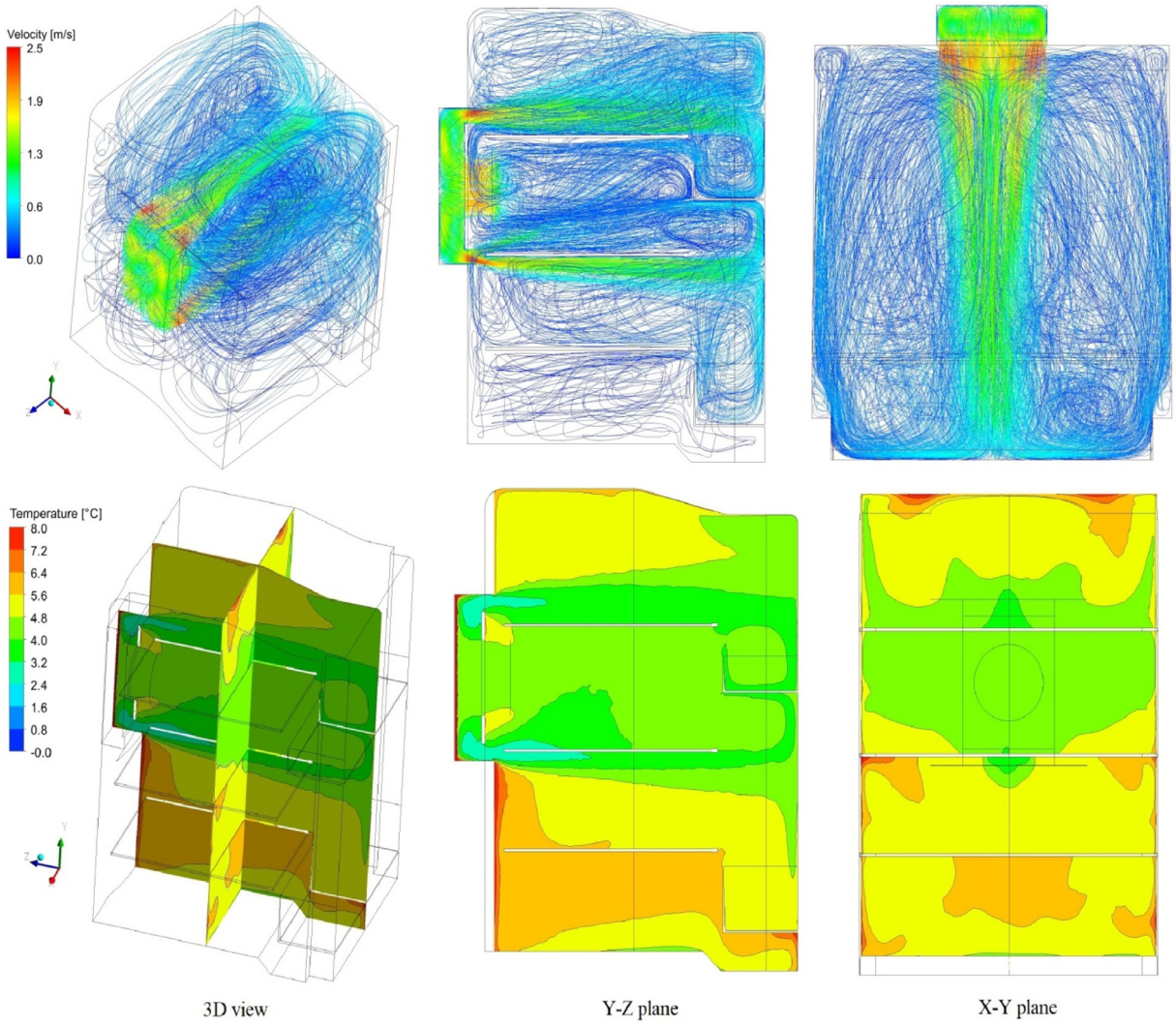

Fig. 11. Air streamlines and temperature distribution for Configuration 5.

Table 11
Energy consumption test results.

Refrigerator	Main supply	Idling voltage		Energy consumption	
	[V]	at 16 °C [V]	at 32 °C [V]	at 16 °C [kW h d^{-1}]	at 32 °C [kW h d^{-1}]
HHR I	24.0	–	–	0.844	3.083
HHR II	20.0	3.5	8.0	0.754	2.285
HHR III	20.0	3.5	8.0	0.759	2.254

sumption test as shown in Fig. 12. As soon as the steady state period was achieved, and the target compartment temperatures indicated in Table 1 were met, the warm packages, which were being kept at an ambient temperature of 25 °C, were inserted into the FFC according the load plan prepared in compliance with the standard. The temperature of the warm packages was 25 °C ± 0.5 °C in the moment of insertion.

The test results for the cooling down time of the HHRs are summarised in Table 12. At a nominal voltage of 24 V, all HHRs have pretty much the same cooling time results. Although more uniform temperature and air flow distribution was achieved by relocating the TEC, this did not affect the cooling time of HHRs II and III. One should also note that, however, the CFD predictions were obtained without the loads, which would definitely affect the air flow inside the FFC.

To decrease the cooling time of HHR II and III, the tests were carried out with the main supply of 24 V and 26.5 V. As seen from Table 12, the lowest cooling time was observed at 24 V and a slight decrease was achieved with 26.5 V. At 20 V, despite increase in the energy efficiency, the cooling time of the HHRs increases.

Table 12
Test results for cooling time.

Refrigerator	Main supply [V]	Idling voltage (16 °C/ 32 °C) [V]	Cooling time [min]
HHR I	24.0	–	146.6
HHR II	20.0	3.5/8.0	164.5
	24.0		146.5
	26.5		142.1
HHR III	20.0	3.5/8.0	165.4
	24.0		144.7
	26.5		139.5

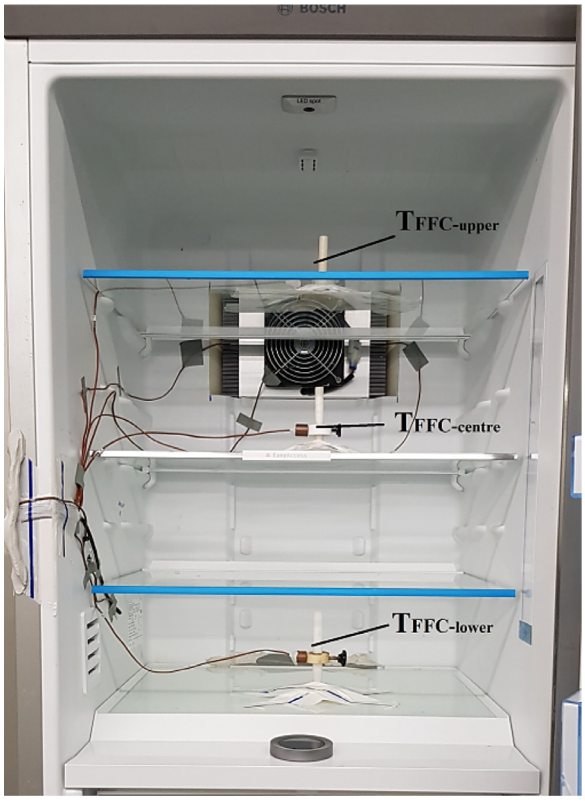

Fig. 12. Location of temperature sensors in the HHR II's FFC.

6. Conclusions

The effect of the current commercial TEC on a household refrigerator was investigated. In the previous study (Soylemez et al., 2018), the TEC was placed into the door of HHR I's FFC and detailed experimental analysis was carried out. The required data for the validation of the CFD predictions was collected for further improvements. In the new study, numerical analysis was first conducted to simulate the optimum location for the TEC. According to the results of the CFD analysis, two new HHRs, HHR II and III, were constructed. Secondly, further improvements were experimentally investigated with HHR II and III, and the tests were performed with their final configurations.

More uniform air and temperature distribution in the FFC of HHR II and III were provided by CFD analysis. In addition to this, considerable increase in the energy efficiency of HHR II and III were achieved by means of key improvement steps. These were the optimisation of the temperature hysteresis inside the FFC (TEC hysteresis), the main and idling voltages (IVs) supplied to the TEC and compressor speeds were optimised in the given order.

In terms of the results, it can be noted that HHR II and HHR III have almost identical energy consumption levels; the differences in their measurements at 16 °C and 32 °C are 0.7% and 1.5%, respectively. An impressive gain was achieved in their energy efficiency by up to 10% and 27% at the ambient temperatures of 16 °C and 32 °C, respectively, compared to HHR I. Considering cooling time, no effect of relocation of the TEC was observed because at 24 V all the HHRs have the same cooling time levels.

The IEC62552:2015 standard is going to be considered as reference standard in most of the countries around the world in the near future. Since the energy consumption test must be performed at two different room temperatures (in most of the current standards, the energy consumption tests are performed at a single room temperature) and a new test of cooling capacity test has been introduced, the TECs will be forced to operate under different conditions much like real operating conditions at end-users. Hence, it is vital to operate the TECs flexibly by supplying them different voltages under various operating conditions to ensure energy efficiency and high cooling performance.

Acknowledgments

This work is funded by the Commission of Scientific Research Projects (BAPKO) of Marmara University under the grant number FEN-C-DRP-130116-0010. Authors also thank BSH Bosch R&D Centre of Refrigeration for providing test chambers and measurement instruments.

References

Ben Amara, S., Laguerre, O., Charrier-Mojtabi, M.-C., Lartigue, B., Flick, D., 2008. PIV measurement of the flow field in a domestic refrigerator model: comparison with 3D simulations. Int. J. Refrig. 31, 1328–1340.
António, C.C., Afonso, C., 2011. Air temperature fields inside refrigeration cabins: a comparison of results from CFD and ANN modelling. Appl. Therm. Eng. 31, 1244e1251.
Astrain, D., Aranguren, P., Martinez, A., Rodriguez, A., Perez, M.G., 2016. A comparative study of different heat exchange systems in a thermoelectric refrigerator and their influence on the efficiency. Appl. Therm. Eng. 103, 1289–1298.
Astrain, D., Martinez, A., Rodriguez, A., 2012. Improvement of a thermoelectric and vapour compression hybrid refrigerator. Appl. Therm. Eng. 39, 140–150.
Astrain, D., Vian, J., Albizua, J., 2005. Computational model for refrigerators based on Peltier effect application. Appl. Therm. Eng. 25, 3149–3162.
Avcı, H., Kumlutas, D., Özer, Ö., Özşen, M., 2016. Optimisation of the design parameters of a domestic refrigerator using CFD and artificial neural networks. Int. J. Refrig. 67, 227–238.
Bansal, P., Martin, A., 2000. Comparative study of vapour compression, thermoelectric and absorption refrigerators. Int. J. Energy Res. (24) 93–107.
Bayer, O., Oskay, R., Paksoy, A., Aradag, S., 2013. CFD simulations and reduced order modeling of a refrigerator compartment including radiation effects. Energy Convers. Manag. 69, 68–76.
Belman-Flores, J., Gallegos-Muñoz, A., 2016. Analysis of the flow and temperature distribution inside the compartment of a small refrigerator. Appl. Therm. Eng. 106, 743–752.
Belman-Flores, J., Gallegos-Muñoz, A., Puente-Delgado, A., 2014. Analysis of the temperature stratification of a no-frost domestic refrigerator with bottom mount configuration. Appl. Therm. Eng. 65, 299–307.
Çengel, Y.A., 2006. Heat and Mass Transfer a Practical Approach, third ed. McGraw-Hill, Singapore.
Ding, G.-L., Qiao, H.-T., Lu, Z.-L., 2004. Ways to improve thermal uniformity inside a refrigerator. Appl. Therm. Eng. 24, 1827–1840.
Fukuyo, K., Tanaami, T., Ashida, H., 2003. Thermal uniformity and rapid cooling inside refrigerators. Int. J. Refrig. 26, 249–255.
Fraisse, G., Ramousse, J., Sgorlon, D., Goupil, C., 2013. Comparison of different modeling approaches for thermoelectric elements. Energy Convers. Manag. 65, 351–356.
Gao, F., Naini, S.S., Wagner, J., Miller, R., 2017. An experimental and numerical study of refrigerator heat leakage at the gasket region. Int. J. Refrig. 73, 99–110.
Gupta, J., Gopal, M.R., Chakraborty, S., 2007. Modeling of a domestic frost-free refrigerator. Int. J. Refrig. 30, 311–322.
Hadidi, A., 2017. A novel approach for optimization of electrically serial two-stage thermoelectric refrigeration systems using chemical reaction optimization (CRO) algorithm. Energy 140, 170–184.
Hermes, C.J., Barbosa, J.R., 2012. Thermodynamic comparison of Peltier, Stirling, and vapor compression portable coolers. Appl. Energy 91, 51–58.
IEC-62552:2015, 2015. *IEC 62552:2015 Household Refrigerating Appliances – Characteristics and Test Methods*, basım yeri bilinmiyor: International Electrotechnical Commission (IEC).
Jugsujinda, S., Vora-ud, A., Seetawan, T., 2011. Analyzing of thermoelectric refrigerator performance. Procedia Eng. 8, 154–159.
Kim, C.N., Kim, J., 2015. Numerical examination of the performance of a thermoelectric cooler with eltier heating and cooling. J. Electron. Mater. 44 (10), 3586–3591.
Kumlutas, D., Karadeniz, Z.H., Avcı, H., Özşen, M., 2012. Investigation of design parameters of a domestic refrigerator by artificial neural networks and numerical simulations. Int. J. Refriger. 35, 1678–1689.
Laguerre, O., Amara, S.B., Moureh, J., Flick, D., 2007. Numerical simulation of air flow and heat transfer in domestic refrigerators. J. Food Eng. 81, 144–156.
Laguerre, O., Benamara, S., Flick, D., 2010a. Numerical simulation of simultaneous heat and moisture transfer in a domestic refrigerator. Int. J. Refrig. 33, 1425–1433.
Laguerre, O., Benamara, S., Flick, D., 2010b. Study of water evaporation and condensation in a domestic refrigerator loaded by wet product. J. Food Eng. 97, 118–126.

Ledesma, S., Belman-Flores, J., 2017. Mathematical application to analyze the thermal behavior of a domestic refrigerator: Influence of the location of the shelves. Int. J. Refrig. 74, 362–370.
Martinez, A., Astrain, D., Rodriguez, A., Aranguren, P., 2016. Advanced computational model for Peltier effect based refrigerators. Appl. Therm. Eng. 95, 339–347.
Martinez, A., Astrain, D., Rodriguez, A., Perez, G., 2013. Reduction in the electric power consumption of a thermoelectric refrigerator by experimetal optimization of the temperature controller. J. Electron. Mater. 42 (7), 1499–1503.
Min, G., Rowe, D.M., 2006. Experimental evaluation of prototype thermoelectric domestic-refrigerators. Appl. Energy 83, 133–152.
Perez-Aparicio, J., Palma, R., Taylor, R., 2012. Finite element analysis and material sensitivity of Peltier thermoelectric cells cooler. Int. J. Heat Mass Transf. 55, 1363–1374.
Riffat, S., Omer, S., Ma, X., 2001. A novel thermoelectric refrigeration system employing heat pipes and a phase change material: an experimental investigation. Renew. Energy 23, 313–323.
Soylemez, E., Alpman, E., Onat, A., 2018. Experimental analysis of hybrid household refrigerators including thermoelectric and vapour compression cooling systems. Int. J. Refrig. 95, 93–107.
Todorov, G., Kamberov, K., Semkov, M., 2017. Thermal CFD study and improvement of table top fridge evaporator by virtual prototyping. Case Stud. Therm. Eng. 10, 434–442.
Vian, J., Astrain, D., 2009a. Development of a hybrid refrigerator combining thermoelectric and vapor compression technologies. Appl. Therm. Eng. 29, 3319–3327.
Vian, J., Astrain, D., 2009b. Development of a thermoelectric refrigerator with two-phase thermosyphons and capillary lift. Appl. Therm. Eng. 29, 1935–1940.
Yamanashi, M., 1996. A new approach to optimum design in thermoelectric cooling systems. J. Appl. Phys. 80 (9), 5494–5502.
Yang, K.-S., Chang, W.-R., Chen, I.-Y., Wang, C.-C., 2010. An investigation of a top–mounted domestic refrigerator. Energy Convers. Manag. 51, 1422–1427.
Zhang, C., Lian, Y., 2014. Conjugate heat transfer analysis using a simplified household refrigerator model. Int. J. Refrig. 45, 210–222.